IEEE Access
Multidisciplinary ⋮ Rapid Review ⋮ Open Access Journal

Received April 15, 2020, accepted April 26, 2020, date of publication April 29, 2020, date of current version May 14, 2020.

Digital Object Identifier 10.1109/ACCESS.2020.2991350

A 10:1 Bandwidth Cryogenic Quadruple-Ridged Flared Horn Design for Reflector Antennas in Radio Astronomy

YUE MA[1,5], CHAN HWANG SEE[2], (Senior Member, IEEE), FENG PANG[1], DI WU[1], DONGLIANG LIU[1], ZUHAIRIAH ZAINAL ABIDIN[3], SIMEON KEATES[2], BO PENG[1], AND RAED A. ABD-ALHAMEED[4], (Senior Member, IEEE)

[1]CAS Key Laboratory of FAST, National Astronomical Observatories, Chinese Academy of Sciences, Beijing 100101, China
[2]School of Engineering and the Built Environment, Edinburgh Napier University, Edinburgh EH10 5DT, U.K.
[3]Research Center of Applied Electromagnetic, University Tun Hussein Onn, Batu Pahat 86400, Malaysia
[4]Faculty of Engineering and Information, University of Bradford, Bradford BD71DP, U.K.
[5]School of Astronomy and Space Science, University of Chinese Academy of Sciences, Beijing 100049, China

Corresponding authors: Yue Ma (yuema@nao.cas.cn) and Chan Hwang See (c.see@napier.ac.uk)

This work was supported in part by the Chinese Academy of Sciences (CAS) Scholarship, in part by the National Natural Science Foundation of China (NSFC) under Grant 11773042 and Grant U1931125, in part by the National Key Research and Development Program of China under Grant 2018YFA0404703, in part by the Open Project Program of the Key Laboratory of FAST, NAOC, and Chinese Academy of Sciences, in part by the Chinese Academy of Sciences (CAS), and in part by the Max-Plank Society (MPG) in the Framework of LEGACY Cooperation on Low-Frequency Gravitational Wave Astronomy under Grant M.IF.A.Radi8098.

ABSTRACT A two port 2.4 to 24 GHz cryogenic Quadruple-Ridged Flared Horn (QRFH) Feed with 10:1 impedance bandwidth is selected for presentation and investigation in this paper. The antenna geometry is formed by using simulation-based optimization which satisfies several stringent design requirements, including impedance bandwidth and radiation characteristics of the proposed antenna. To verify the theoretical performance, a prototype of the optimized QRFH was manufactured and tested. The reflection coefficients of the antenna are below −10 dB and the mutual coupling is better than −25 dB. Meanwhile, the antenna aperture efficiency is above 55% and maximum gain is from 10.5 to 21.1dBi across the desired working frequency band. Both the simulated and measured results exhibit good agreement. To demonstrate the suitability of the proposed design in a practical environment, a prototype Cryogenic system composed of a cryogenic Dewar and a QRFH, has been designed and its performance was measured. The results showed that the physical temperature reached an acceptable level which was less than 45 K. The overall performance of the proposed QRFH feed suggests that it would be applicable to the receivers for the Square Kilometre Array (SKA) reflector antenna, and meets requirements of the SKA advanced instrumentation program (AIP).

INDEX TERMS Quadruple-ridged horn, reflector antenna, cryogenic system, wideband feed.

I. INTRODUCTION

The Square Kilometre Array (SKA) is an unprecedented telescope program that will support a wide spectrum of key science goals in cosmology and galaxy evolution, fundamental physics, and astrobiology. It will enable scientists to receive signals of approximately one million square metres of collecting area, which could extend to 3000 kilometers baseline from a central core region with a series of spiral structures across southern Africa and western Australia. This significant increase in scale compared with existing telescopes requires a revolutionary advancement from traditional radio telescope design. The SKA is a joint venture involving more than 10 countries, including China. The combined radio instrument will make hundreds of thousands of radio telescopes, with three antenna arrays, such as a low-frequency aperture array from 50 MHz to 350 MHz, a mid-frequency aperture array from 400 MHz to 1.7 GHz and a dish array from 350 MHz to at least 20 GHz. In case of the dish array, the first phase of the SKA is expected to involve building 133 dishes with 15 m aperture in southern Africa from 2021. In the second phase of the SKA, the dish array will be expanded

The associate editor coordinating the review of this manuscript and approving it for publication was Lu Guo.

to approximately 2500 dishes after 2030, which will enable high sensitivity, high survey speed, wide frequency bands and a very large effective collecting area [1], [2].

The key science goals of the SKA project are in place and well-structured, with the detailed design and preparation for the global technology development program ongoing. Currently, the JLRAT/CETC54 (Joint Laboratory for Radio Astronomy Technology, National Astronomical Observatories, Chinese Academy of Sciences & the 54th Research Institute of China Electronics Technology Group Corporation) completed two SKA dish prototypes. One is located in Shijia Zhuang, Hebei Province, China. Another has been transported to southern Africa [1]. To keep abreast with this development trajectory, reflector feed designs for decade-bandwidth radio telescopes have been investigated intensively by antenna designers and RF microwave engineers globally. To this end, several types of feed design such as the Quadruple-Ridged Flared Horn (QRFH) feed [3]–[10], the Eleven feed [6], [11], the Sinuous feed [6], [12] and the Quasi Self-Complementary (QSC) feed [6], [13], have been proposed, investigated and implemented. Eleven Feed [11] offers attractive constant beamwidth and phase centering on its radiation pattern characteristics and good 7:1 wide impedance bandwidth, but suffers from requiring additional circuitry to match and differentially feed its 200 Ω input impedance, and a comparatively high manufacturing cost. Sinuous Feed [12] has stable radiation patterns and lower fabrication cost than its counterparts. However, it suffers from narrower 4:1 impedance bandwidth. QSC [13] has the same deficiencies as well as poor high frequency performance, but it has a broader 1:10 impedance bandwidth. In contrast to all the above, QRFH Feed [13] has all the good features of its counterparts and it also has a 50 Ω desired input impedance. This means that it does not acquire any additional circuitry for its feeding network.

To complement the above feed design, the wideband single pixel feed (WBSPF) which is one of the SKA's three advanced instrumentation programs (AIP) in the pre-construction phase of the SKA project, was proposed [1]. The WBSPF aims to greatly extend the bandwidths of the radio astronomical receivers beyond conventional broadband octave receivers while maintaining the same sensitivity criteria. It is desired that the number of receivers required for future large radio telescope arrays will be reduced, thus lowering the fabrication cost and enabling instantaneous wide frequency range observations [3], [10]. For a wideband radio telescope, it must have a very low system noise temperature [10] to achieve the highest possible sensitivity. In addition to the noise from the external environment, the receiver link of the radio telescope inevitably produces noise. Therefore, radio telescopes not only need to carefully design the feed, but also often reduce the internal noise of the system through refrigeration. According to WBSPF baseline of an internal report for Cryogenic feed, to reduce the ohmic loss to 0.08 dB, the physical temperature needs to be cooled to less than 50 K, and the estimated noise temperature for feed should be less than 0.94 K [1], [14]. This design criterion imposes further challenges in designing the SKA feed.

The configuration of a QRFH can be described as a flared quad-ridged waveguide. It could also be considered as a quad-ridged antenna wrapped by a smooth-wall horn. By optimizing the QRFH's profile, the freedom of controlling the beamwidth and its desired metal structure can be achieved. Due to the inherent characteristics of QRFH, such as multi-octave bandwidth, dual linear polarization, 50 Ω input impedance and good radiation characteristics, this has motivated researchers to come out with many improved and modified designs over past decade [3]–[10], [15]–[21]. However, on examining these published works [3]–[10], [15]–[21], they were in low-frequency ranges (below 20 GHz), have less impedance bandwidth and did not investigate the performance of QRFH with a cooling system. To address this knowledge gap, this paper presents a modified QRFH feed design operating from 2.4 to 24 GHz with 10:1 impedance bandwidth. To demonstrate that the proposed QRFH meets the low noise temperature and has a better sensitivity, the QRFH was tested and integrated with a cryostat to form a cryogenic receiver system for a radio telescope.

The overall 3D prototype of the QRFH has an aperture diameter of 170 mm ($1.36\lambda_{2.4GHz}$) and a height of 187.2 mm ($1.5\lambda_{2.4GHz}$). For such a complex shape, the whole model will be described in Section II. Simulated and measured results for QRFH are presented in Section III. Measurements of the physical temperature for Cryogenic Quadruple-Ridged Flared Horn Feed and predicted system performance of the feed for radio telescope are shown in Section IV. Conclusions are drawn in Section V.

II. ANTENNA DESIGN

The detailed structure and the parameters of Quadruple-Ridged Flared Horn Feed are presented in this section along with its dimensions.

A. THE STRUCTURE OF THE QUADRUPLE–RIDGED FLARED HORN FEED

The novel QRFH feed is designed in three main sections, as shown in Fig.1, i.e. horn, ridge waveguide and straight waveguide. The aperture and length of the horn determine the radiation characteristics of the dual-polarized horn antenna. The horn section includes a smooth sidewall, which is seated outside, along with four ridges, which are located inside. The ridge structure works as a guide, where the electromagnetic energy from the ridged waveguide is concentrated in the middle region of the ridges and transmitted to the aperture of the horn surface. The characteristic impedance of ridged waveguide feed port is 50 Ω and aperture of the horn surface is 377 Ω. The ridge structure usually uses exponential gradient to smooth the impedance in the transformation process. From the feeding point to the bottom mouth of the conical horn is a four-ridged circular waveguide section. The quadruple-ridged circular guide has been

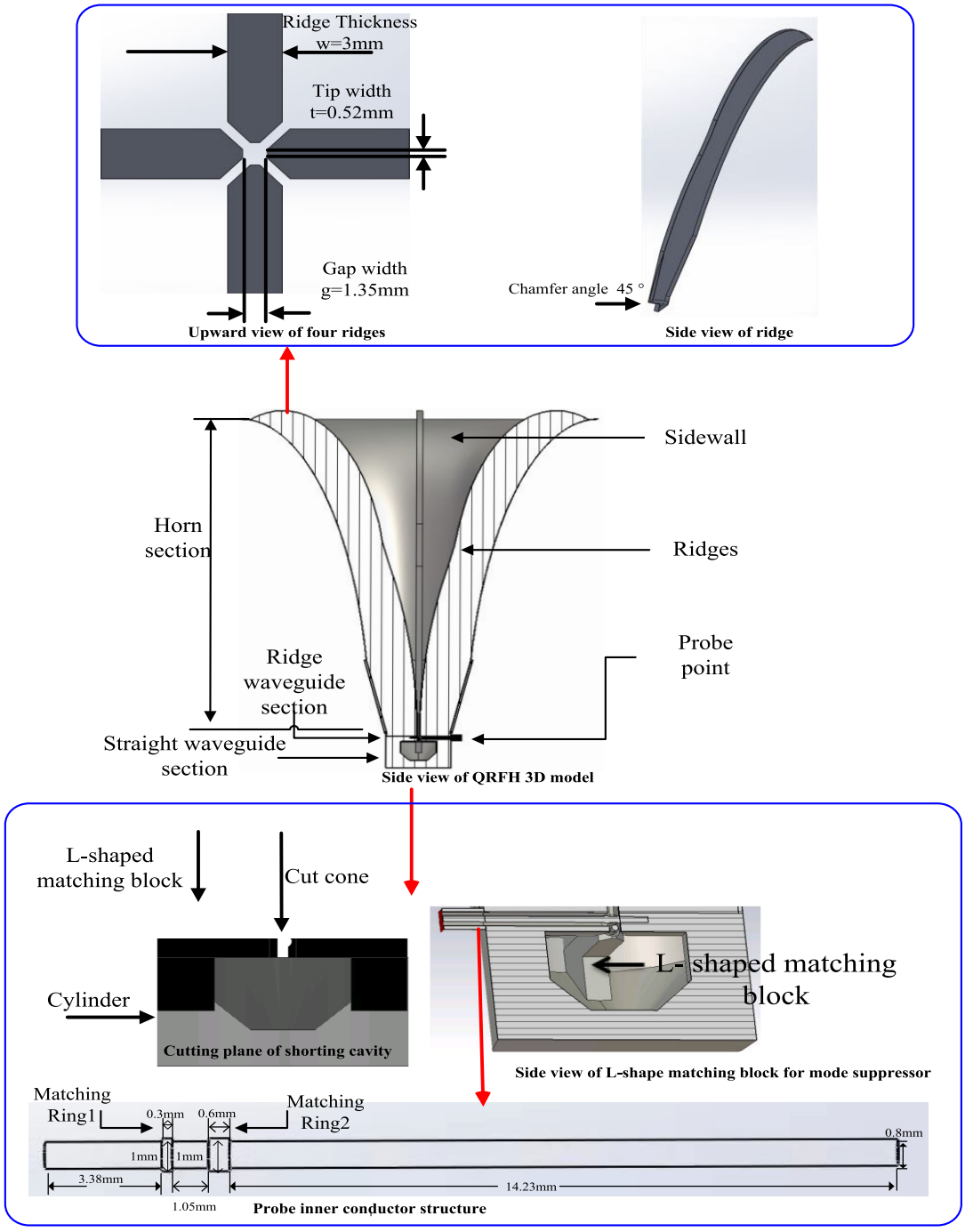

FIGURE 1. Detailed view of QRFH.

commonly considered as a very wide-band radiator. It is mainly used to reduce the cutoff frequency for the fundamental mode of transmission signal and increase the available bandwidth [22]. To provide a dual-polarization capability, a circular waveguide as a radiator could be used because it can support two orthogonal modes [23].

The complex structures of the proposed antenna are depicted in Fig.1. The aperture of conical horn is 170 mm and the height is 168.5 mm, while the aperture of the ridged circular waveguide is 31 mm and the height is 1 mm. As can be seen, the bottom of the QRFH section is a shorting cavity, which is formed by a cylinder, a cut cone and an L-shaped matching block for impedance matching. The cylinder has an aperture and height of 31 mm and 18.7 mm respectively, while a cone cut from cavity has upper and lower apertures, and height of 31 mm, 8 mm and 11.3 mm, respectively.

The L-shaped block is 48 mm long, has bending size of 10 mm × 6.97 mm with 3 mm thickness.

The dimensions of the four ridges can be viewed from the top of the structure as illustrated in Fig.1. The ridge has a thickness of 3mm, tip width of 0.52 mm with a ridge gap of 1.35mm. The chamfer angle of 45 degree can be observed from the side view of the ridge.

As for the feeding part of the antenna, it is designed with two orthogonal probes and its inner conductor structure is also shown in Fig.1. It is noticeable that the inner conductor is matched by five cylinder matching segments and the dimension of each section can be found in Fig.1. A 3D QRFH prototype was manufactured in aluminum and is shown in Fig.2.

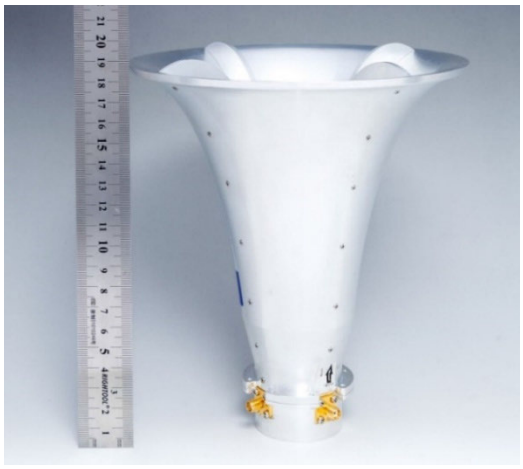

(a) Front view of QRFH

(b) Top view of QRFH

(c) Bottom view of QRFH

FIGURE 2. Prototype photograph of the QRFH.

B. THE PARAMETRIC STUDY OF THE QUADRUPLE-RIDGED FLARED HORN FEED

To understand the sensitivity of the geometrical parameters of the antenna, the CST(Computer Simulation Technology) [24] was used to carry out the study here. Ridge design has been the most critical element in achieving good performance of the QRFH, including ridge profile, ridge thickness and ridge gap. In this design, the ridge profile was constructed using discrete points from analytical profiles [6]. To understand the effect of ridge profile, ridge thickness, shorting cavity and probe inner conductor structure design on reflection coefficient and radiation patterns, a parametric study has been carried out.

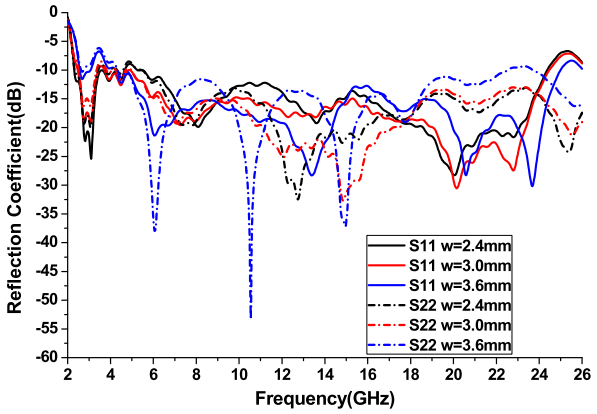

FIGURE 3. The effect of thickness ridge on reflection coefficient.

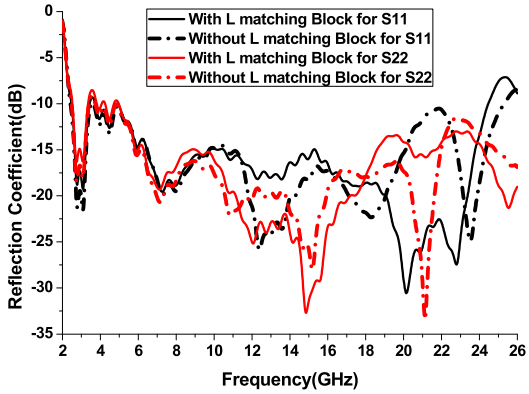

FIGURE 4. L- Shaped matching block effects on reflection coefficient.

Fig.3 shows the effect of ridge thickness (w) on the feed reflection coefficient when changing w from 2.4 mm to 3.6 mm with increment of 0.6 mm. It can be seen that, the S11 will be degraded (higher than -10 dB) at around 3.8 GHz if the thickness of the ridge is thicker (w = 3.6 mm), while the S11 will be deteriorated at 5 GHz and better at 24 GHz if the thickness of ridge is thinner (w = 2.4 mm). In contrast, with thicker w, the S22 will be impaired at both lower frequency band (3.2 to 4.3 GHz) and upper frequency band (18.2 to 24 GHz),while reducing the thickness from 3.6 to 3.0 mm, S22 can be improved to better than -10 dB across all the frequency bands. Fig.4 depicts the vital role of the L-shaped matching block in shorting cavity as an adapter. It can be clearly seen that the improvements of the impedance matching is achieved by using this adapter. In high frequency bands, especially, it could improve 11-20 dB from 20 to 23 GHz for S11 and reach below -10 dB from 22 to 24 GHz for S22. As can be noticed, by incorporating this L-shaped block into the design, it was able to achieve the desired 10:1 bandwidth working frequency bands for dual-polarized QRFH. The probe inner conductor is specially designed with two rings for 50 Ω port matching. Fig.5 depicts

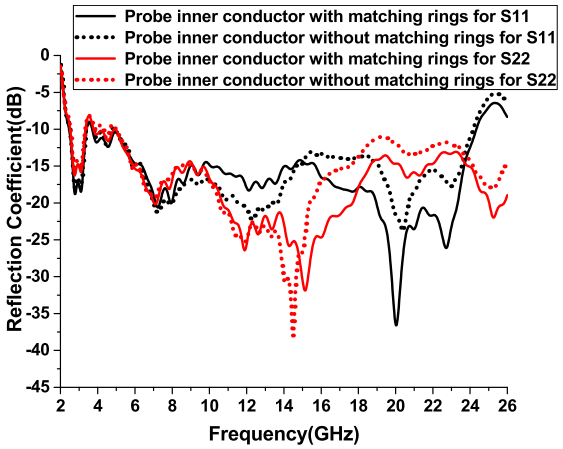

FIGURE 5. Matching rings for probe inner conductor effects on reflection coefficient.

the variation of the reflection coefficient S11 and S22 of the proposed QRFH with and without the matching rings. It is clearly seen that improvements of 1-7 dB from 15 to 24 GHz can be achieved by introducing matching rings in the design.

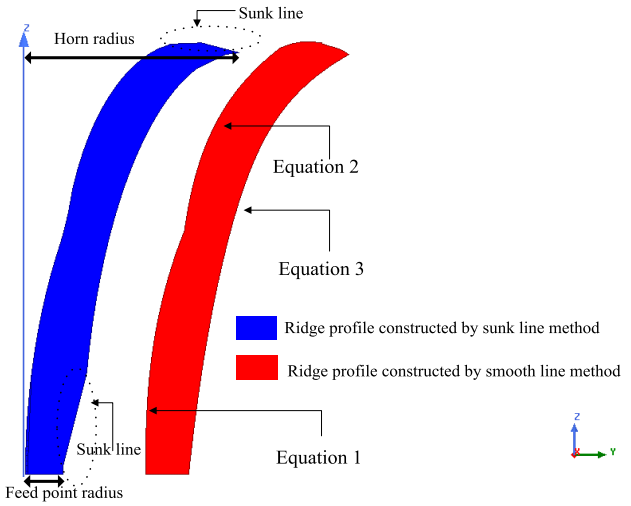

FIGURE 6. Comparisons between sunk line and smooth line for ridge profile.

Many functions are applied in mapping ridge profiles, such as linear, sinusoid, tangential, x^p, exponential and elliptical functions [6]. The profiles of the ridges in this article are determined by sunk line and smooth line methods, which can be seen in Fig.6. For the smooth line, it was constructed by fitting three functions to achieve a continuous line. The sunk line was constructed by using 178 discrete points with antenna performance optimization. Comparing the two methods, the optimization results show that the sunk line method will improve a lot on the stability of phase center performance to reduce fluctuation range from $0.5\lambda_{2.4GHz}$ to $0.2\lambda_{2.4GHz}$. Fig.7 illustrates the calculated phase center location with respect to the aperture of sunk profile QRFH feed, the distance from 23.96 to 82.87 mm over the operating frequencies,

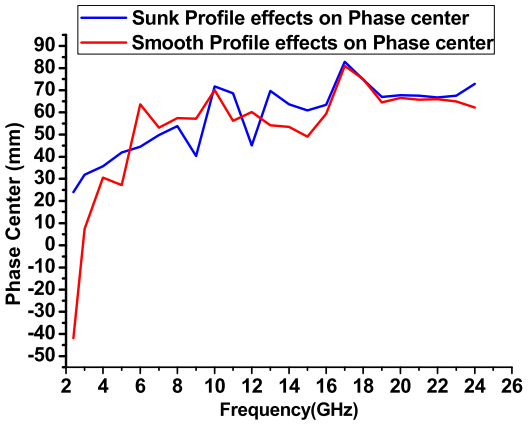

FIGURE 7. Comparisons between sunk profile and smooth profile on phase center.

the maximum fluctuation range is 29.46 mm, (about $0.2\lambda_{max}$, $\lambda_{max} = \lambda_{2.4GHz} = 125$ mm). Therefore, the stability of phase center is acceptable.

Here, functions of the smooth line profile are defined as:

$$Y(z) = a1 \times e^{cz} + a2 \times (d - z)/d + a3 \times (z/d)^m \quad (1)$$

where Y is the vertical distance between the ridge profile and the axial line; z is evaluated value along the axis line; d is length of sidewall; $a1$,$a2$,$a3$ and c, d are the parameters for the adjusted ridge profile; $a1$ and $a2$ principally determine the small distance to the end of ridges; c is the main parameter of ridge curvature adjustment; and, $a3$ and m slightly adjust the ridge profile.

$$\begin{aligned} Y(z) &= C1 \times e^{Rf \times z} + C2 \quad where \\ C1 &= \left(\frac{L}{2} - \frac{a}{2}\right) \times (e^{Rf \times Lm} - 1) \\ C2 &= (\frac{a}{2} \times e^{Rf \times Lm} - \frac{L}{2})/(e^{Rf \times Lm} - 1) \end{aligned} \quad (2)$$

a is the curve of start point diameter; Lm is the length of the curve; L is the end point diameter; and Rf is the curvature.

$$Y(z) = b1 + b2 \times e^{m1 \times z} + b3 \times (z/l1)^Q \quad (3)$$

where Y is the vertical distance between the ridge profile and the axial line, z is evaluated value along the axis line, $l1$ is the length of the sidewall, $b1$,$b2$,$b3$ and $m1$, Q are the parameters for the adjusted ridge profile, and, $b1 + b2$ effects the bottom diameter of the horn feed.

To demonstrate how the above three equations were used to find the QRFH structure, Table 1 shows the final optimized parameters which provides the smooth ridge profile for the QRFH.

It can be seen that when comparing the two methods, Fig.7 shows the sunk line method is better and improves the stability of the phase center performance. Based on using these continuous functions to adjust the number of required discrete points, the feed radiation performance is optimized. It is found that the identified 178 discrete points are good

TABLE 1. Relevant parameter values of three equations for smooth profile.

Parameters	Value	Parameters	Value
a1	0 mm	*C1*	0.0046
c	0 mm	*C2*	-0.0046
d	175 mm	*b3*	22 mm
a3	65 mm	*l1*	170 mm
m	2.5	*b2*	11 mm
L	129 mm	*m1*	9300 mm
Rf	30000 mm	*b1*	6 mm
a	0 mm	*Q*	10
Lm	90 mm	*a2*	0 mm

TABLE 2. Final optimized main parameter values for sunk profile.

Parameters	Value
Horn radius	85 mm
Feed point radius	15.5 mm
Length of sidewall	187.2 mm

enough to meet the required performance, therefore, the values of horn radius, feed point radius, length of sidewall also has been identified as listed in Table 2.

III. SIMULATED AND MEASURED RESULTS

The antenna prototype was assembled by adopting the horn, four ridges and shorting cavity to achieve the required rigidity and symmetry in the structure with 170 mm diameter and 187.2 mm height.

The complex structure was fabricated with aluminum alloy using CNC (computer numerical control) milling technology. To verify the simulated results, a prototype was realized to provide holistic practical evaluation of the design. The detailed measurements of the S-parameters and radiation characteristics of the proposed QRFH are elucidated in this section.

A. S-PARAMETERS

A Rohde & Schwarz ZVA40 vector network analyzer was adopted to measure S-parameters with the horn pointing at free space. Simulated and measured results are plotted below for the two polarizations; S11 and S22 are seen to be below -10 dB across most of the desired working frequency band from 2.4 to 24 GHz, as shown in Fig. 8. Also, as depicted in Fig.9, the simulated and experimental S21 level is mostly lower than -25 dB. The good isolation performance indicates that good decoupling between the ports. It also confirmed that the ridges are precisely aligned and machined in orthogonal planes, demonstrating the success of combining the three sections of the structure.

B. RADIATION PATTERNS

The radiation characteristics of the proposed antenna were measured in an anechoic chamber, and are illustrated in Fig.10. Two gain reference horns were used to cover the required working frequency spectrum, i.e. a low gain horn for 2.4 to 17 GHz and a high gain horn operating from

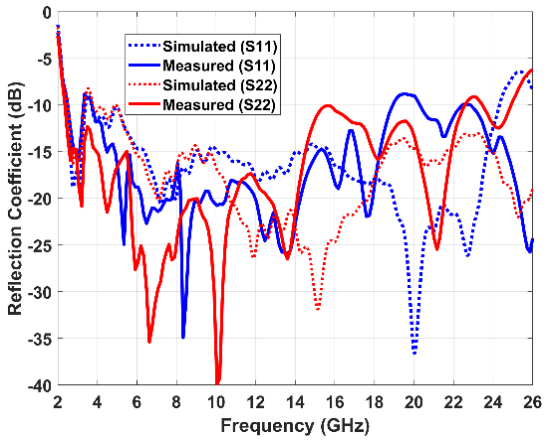

FIGURE 8. Comparison for QRFH S11 and S22 between simulated and measured results.

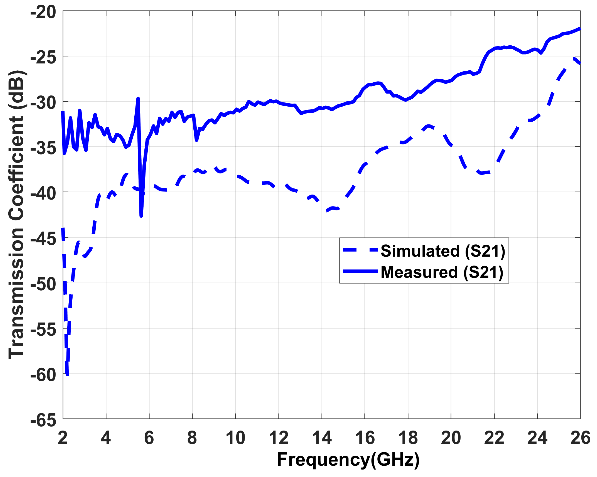

FIGURE 9. The comparison for QRFH S21 between simulated and measured results.

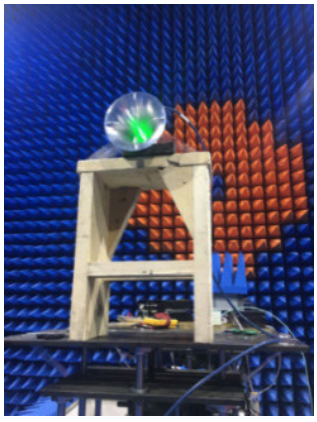

FIGURE 10. Radiation patterns measured in an anechoic chamber.

18 to 24 GHz. Gain was measured by substitution. The radiation patterns of the antenna are depicted in Fig.11. To check the consistency and variations of the patterns across the frequency bands, seven frequency points were selected,

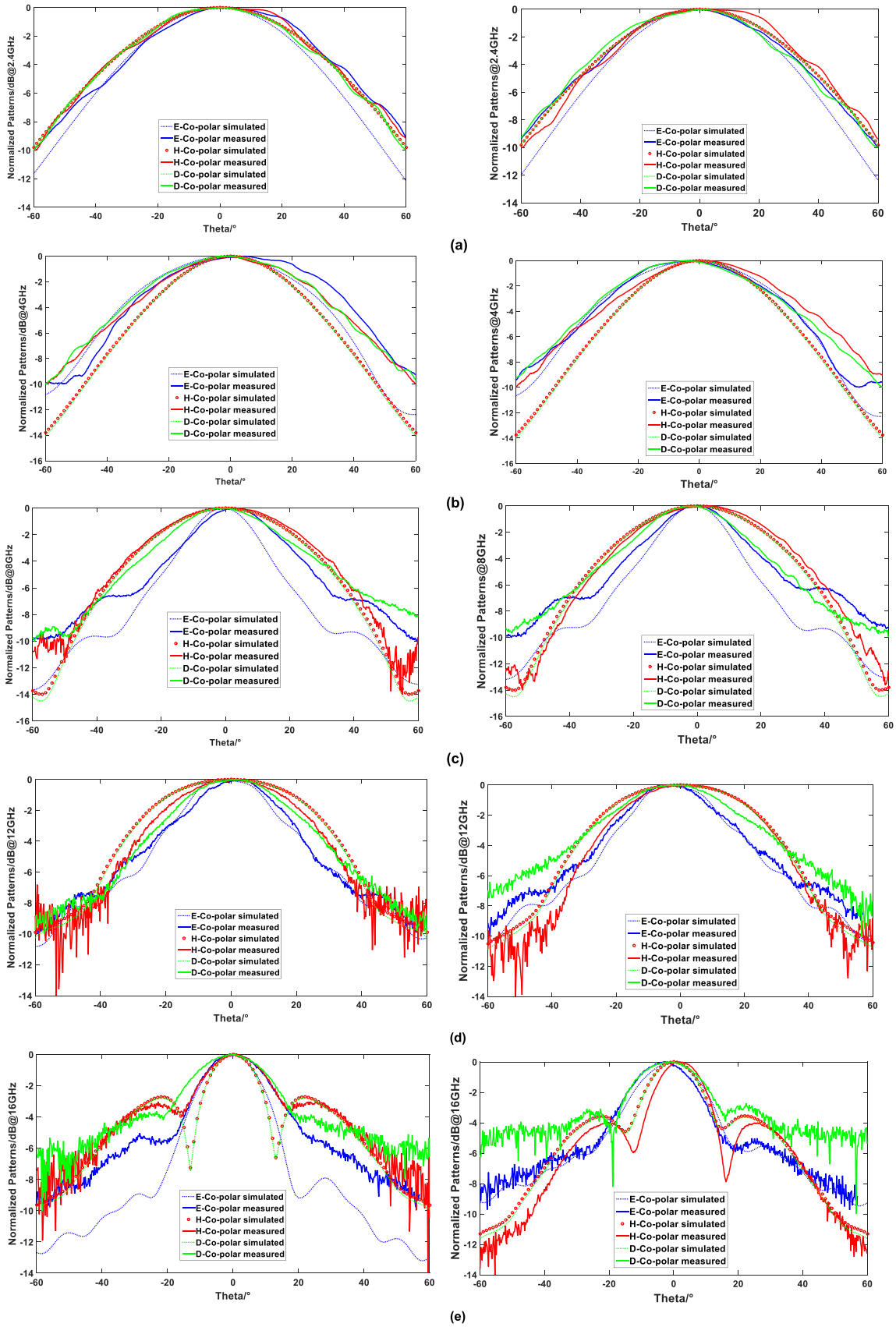

FIGURE 11. Comparisons between simulated and measured radiation pattern for (a) 2.4 GHz, (b) 4 GHz, (c) 8 GHz, (d) 12 GHz, (e) 16 GHz, where left: Port 1 and right: Port 2.

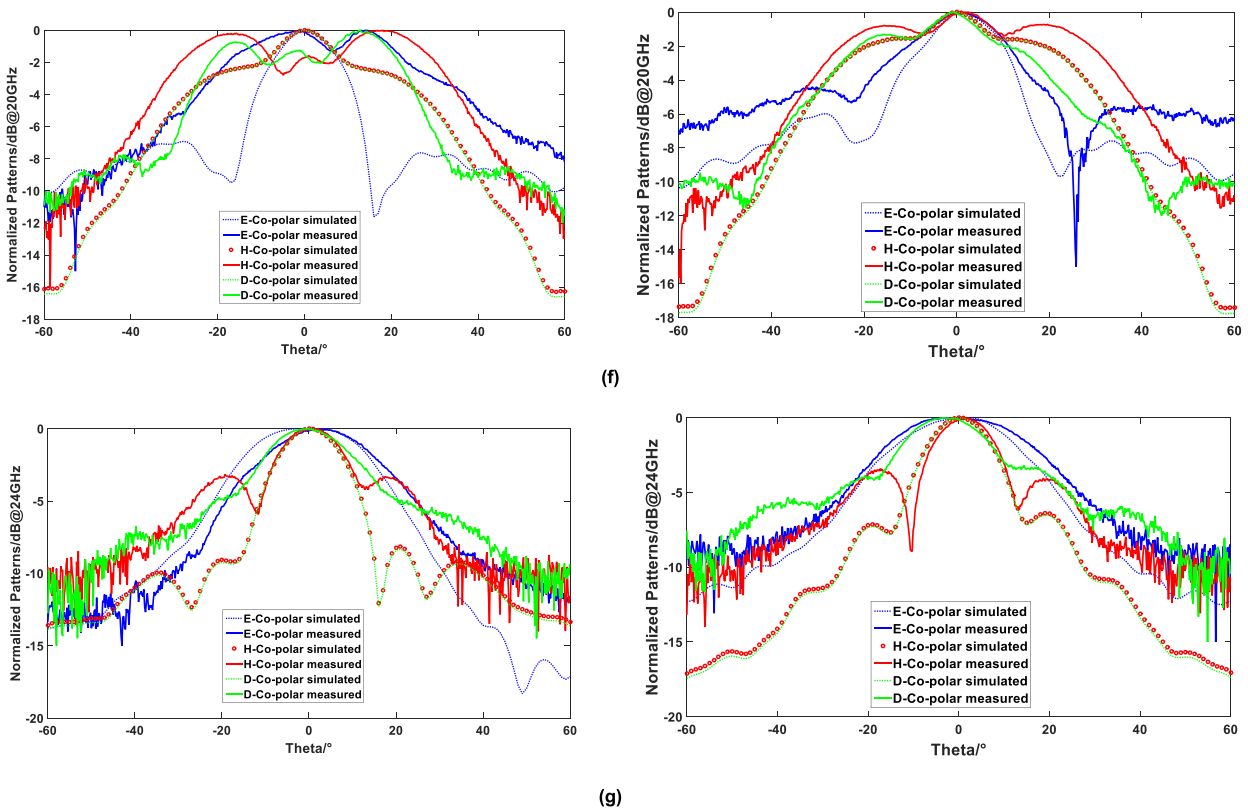

FIGURE 11. ***(Continued.)*** **Comparisons between simulated and measured radiation pattern for (f) 20 GHz, and (g) 24 GHz, where left: Port 1 and right: Port 2.**

i.e. 2.4, 4, 8, 12, 16, 20 and 24 GHz for two ports. Due to the SKA dish antenna possesses shaped offset-Gregorian optics, with 5.2 m for the sub-reflector with subtended angle of $\theta_c = 58°$ [1], [15] and a projected diameter of 15 m for the main reflector only the $\pm 60°$ illumination zone is plotted for the QRFH feed. Fig. 12 compares and plots the simulated results against the measured results of the radiation patterns at -10 dB beamwidth in the E- ($\varphi = 0°$), H- ($\varphi = 90°$) and D- ($\varphi = 45°$) planes, respectively. These three planes offers a clearer picture of the patterns. The measured patterns in the E, H and D-planes demonstrate uniformity across most of the working frequency band. The simulated and experimental maximum gains of the QRFH for two ports are shown in Fig.13 and both results are in good agreement within the range of 10.5 dB to 21.1 dB over the working frequencies.

To evaluate the feed antenna aperture efficiency, GRASP (General Reflector Antenna Software Package) [25] was used to model the feed in SKA dish. This software is the main tool for on-dish simulation using PO (Physical Optics) augmented by the PTD (Physical theory of diffraction) with the reflector illuminated by the designed feed. Fig.14 shows the antenna aperture efficiency over the desired operating frequency band. The efficiency is ranging from 75% to 55% over 2.4 to 24 GHz for the two ports.

C. PERFORMANCE COMPARISON

A comparison between the proposed QRFH feed and other published works, in term of minimum reflection coefficient (S11/S22), minimum mutual coupling (S21), impedance bandwidth, maximum gain, antenna efficiency and antenna size is given in Table 3. It is noticeable that the proposed work has achieved a wider impedance bandwidth with also better S-parameters against the others. The presented design also has comparable size, reasonable antenna gain and acceptable aperture efficiency in comparison with other published works.

IV. PREDICTED CRYOGENIC SYSTEM PERFORMANCE

The designed aperture of the QRFH feed is only 170 mm, which helps to reduce the size of the vacuum window and thermal load, and minimizes the cryostat volume to reduce the overall radiating surface area. An essential aspect of the important aspect cryogenic feed design is to assess its performance when it is placed inside the cryostat and being cooled down to the baseline requirement temperature of 45 K which meets the target of less than 50 K [1], [14].

A. CONFIGURATION AND MEASURE ENVIRONMENT FOR CRYOGENIC QRFH

A minimized Dewar has been designed for the 10:1 bandwidth QRFH, and is shown in the Fig.15. The cryogenic system includes a Vacuum Window (Mylar) [26], [27], Dewar Cavity, Feed, Thermal Shield, and G10 Supporter which is a glass fiber and resin rolled composite material supporter. The cryogenic temperature performance has been both estimated and measured on the mechanical and cryogenic

TABLE 3. Comparisons of Feed performance between the published works and the proposed work.

Feed Type	Working Frequency and bandwidth	S11/S22	S21	Maximum gain	Antenna efficiency	Size (Aperture diameter, height)
Dong's design [7]	4.6-24 GHz (5:1)	-8 dB	-21dB	N/A	53%	$(3.1\lambda_o, 2.8\lambda_o)$
Shi's design [8]	8-50 GHz (6:1)	-7dB	-20dB	N/A	60%	$(1.54\lambda_o, 1.17\lambda_o)$
Jonas's design[15]	1.5-4.5 GHz (3:1)	-10 dB	-40dB	N/A	68%	$(1.2\lambda_o, 1.2\lambda_o)$
Akgiray's design [5]	2.5-11GHz (3:1)	-15dB	-30dB	7-14dBi	50%	$(1.14\lambda_o, 1.09\lambda_o)$
Mallahzadeh's design[16]	8-18 GHz (2:1)	-9.45dB	-21dB	10-16.2dBi	N/A	$(1.69\lambda_o, 2.05\lambda_o)$
Billade's design[9][15]	0.35-1.05 GHz (3:1)	-10dB	-35dB	10.6-13dBi	66%	$(1.16\lambda_o, 1.16\lambda_o)$
Bekir's desogn [17]	1-6.75 GHz (6.75:1)	-10dB	-28dB	13.6-18.1 dBi	N/A	$(1.87\lambda_o, 2.1\lambda_o)$
Yang's design[18]	1-6 GHz (6:1)	-10dB	-35dB	N/A	50%	$(5\lambda_o, 0.33\lambda_o)$
Jonas's dielectric design[19]	1.5–15.5 GHz (10.3:1)	-7dB	-35dB	6.5-12.5dBi	50%	$(1.9\lambda_o, 0.58\lambda_o)$
Proposed work	2.4-24 GHz (10:1)	-10 dB	-25 dB	10.5-21.1dBi	55%	$(1.36\lambda_o, 1.5\lambda_o)$

*λ_o is the lowest operating frequency

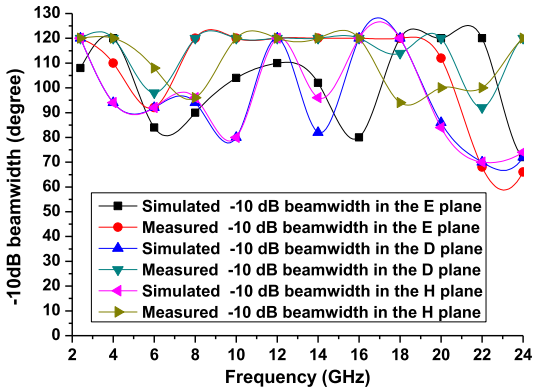

(a)

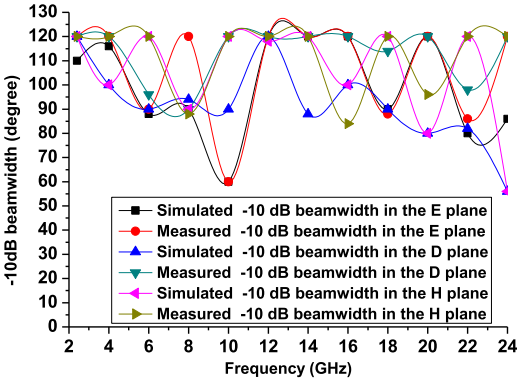

(b)

FIGURE 12. -10 dB beamwidth comparisons between simulated and measured results on three different planes for (a) port1 and (b) port2.

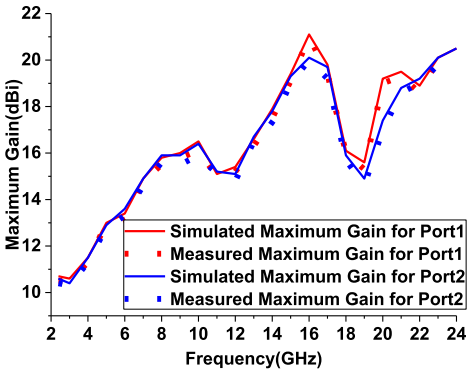

FIGURE 13. Simulated and measured maximum gains of the QRFH Feed.

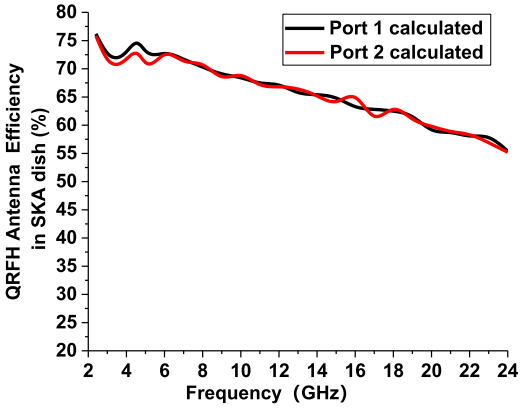

FIGURE 14. The Antenna aperture efficiency in SKA dish was calculated with two ports.

Dewar systems. The configuration of the completed measurement is presented in the block diagram in Fig.16. The cryogenic Dewar system consisteds of nine main parts: Temperature Monitor, Vacuum Gaug, Vacuum Pump,Vacuum Pipe, Helium Compressor, Helium Pipe, Cold Heading, Cryogenic Dewar and feed. In this cooling environment, it is noted

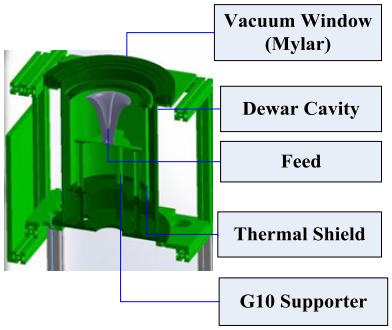

FIGURE 15. 3-D structure with mechanical design for Cryogenic.

TABLE 4. The main equipment list.

Equipment Name	Model Number
Cold Head	KDE210SA*
Helium Compressor	M600
Compound vacuum gauge	ZDF-III-LED
Temperature Monitor	M9308

KDE210SA* is two-stage of refrigerator cold head, which was designed by CSIC [28]

TABLE 5. Temperature sensors details in the Dewar.

Temperature Sensor Location	Temperature Sensor code with measured value
2nd stage cold plate	17100-1719-F 8 K
	15093-1110-B 8 K
Feed	15088-2123-D 46 K
	17043-4307-C 45 K
1st stage cold head	15077-4142-E 38 K
Thermal Shield	15092-3029-A 207 K
	17041-4645-G 207 K

that the Vacuum Gauge,Vacuum Pump and Vacuum Pipe are used to measure the internal vacuum of the Dewar cavity, while the Helium Compressor, Helium Pipe and Cold Head are used for cooling. Moreover, the temperature monitor with series temperature sensors is used to measure the physical temperature, whereas the Dewar Cavity is used to support a Vacuum sealing environment. Table 4 lists the main equipments used in the measurement, as shown in Fig.16.

B. MEASURED HEAT FOR 10:1 BANDWIDTH FEED REFRIGERATOR

After 24 hours' cooling, the monitored temperature sensor displayed the feed physical temperature as less than 50 K, as shown in Fig.17. This indicates that the WBSPF performance requirements have been achieved when the temperature can keep at 45 K and the final vacuum degree is $4.0\text{x}10^{-5}$ Pa. When the vacuum degree is better than 10^{-5} Pa, the convection heat can be neglected [26].

From the temperature monitor (refer to Fig. 18 blue points), it can be clearly noticed that the temperature on the Thermal Shield is 207 K, the temperature on the 2nd stage of the Refrigerator cold head is 8 K, the 1st stage of the Refrigerator cold head is 38 K, the temperature on the Feed plate is 45 or 46 K. According to the above measured different sections of temperature and KDE210SA thermal conductivity curve [28], the measured heat on the 2nd stage of the Refrigerator cold head is 3 W, and 1st stage of Refrigerator cold head is 37 W. Here, the QRFH is only connected to the 1st stage of the Refrigerator cold head by copper strips, so the thermal load on the 1st stage of Refrigerator cold head needs to be considered.

C. THEORY CALCULATION VERIFICATION ON 10:1 BANDWIDTH FEED REFRIGERATOR HEAT

In order to evaluate the required refrigerating capacity, the conductive and radiant loading to be absorbed by the first and second stages of the refrigerating head must be estimated by the system designer. Due to convection, there is a third heat load which causing by heat conducted from the Dewar walls to the cold head by the residual gas inside Dewar. When the vacuum quality is good, the third heat load can be neglected. Therefore, this is not taken into account in estimating the total heat load. Finally, the heat is coming from the conductive and radiation load [26]. There is no conductive heat and radiation loading on the 2nd stage of the Refrigerator cold head for QRFH experiment. This is due to the 2nd stage of the Refrigerator cold head being mainly used for cooling the LNA (low-noise amplifier) device.

1) ESTIMATING THERMAL LOAD DUE TO CONDUCTION

$$H = \frac{A}{L}\int_{t1}^{t2} K dt \tag{4}$$

where:

H =heat
A = cross section area of the conducting element in m^2
L = the conducting elements length in m
K = the thermal conductivity in $Wm^{-1}K^{-1}$.
T_1 = the colder temperature in K
T_2 = the warmer temperature in K

Here, for cryogenic feed, G10 supporter, $K = 0.34$ W/mK is chosen [26]. The sources of conductive heat are the 1st stage of the Refrigerator cold head and the 2nd stage of the Refrigerator cold head. All the area of surfaces is estimated using Solid Works software.

$$\text{1st stage} \quad H_{Conduction} = H_1 + H_2 \tag{5}$$

H_1 is the conductive heat from the 300 K baseplate of the Dewar to the 207 K baseplate of the thermal shield.

H_2 is the conductive heat from the 207 K baseplate of the thermal shield to the 45 K baseplate of the feed. The temperature on the baseplate of the Dewar is 300 K and the baseplate of the thermal shield is 207 K. There are four G10 supporters used in this work with the inner diameters of 20 mm, the outer diameter is 24 mm and the height is 136 mm. By using Eq.(4), the value of conductive heat for H_1 can be calculated as 0.112 W.

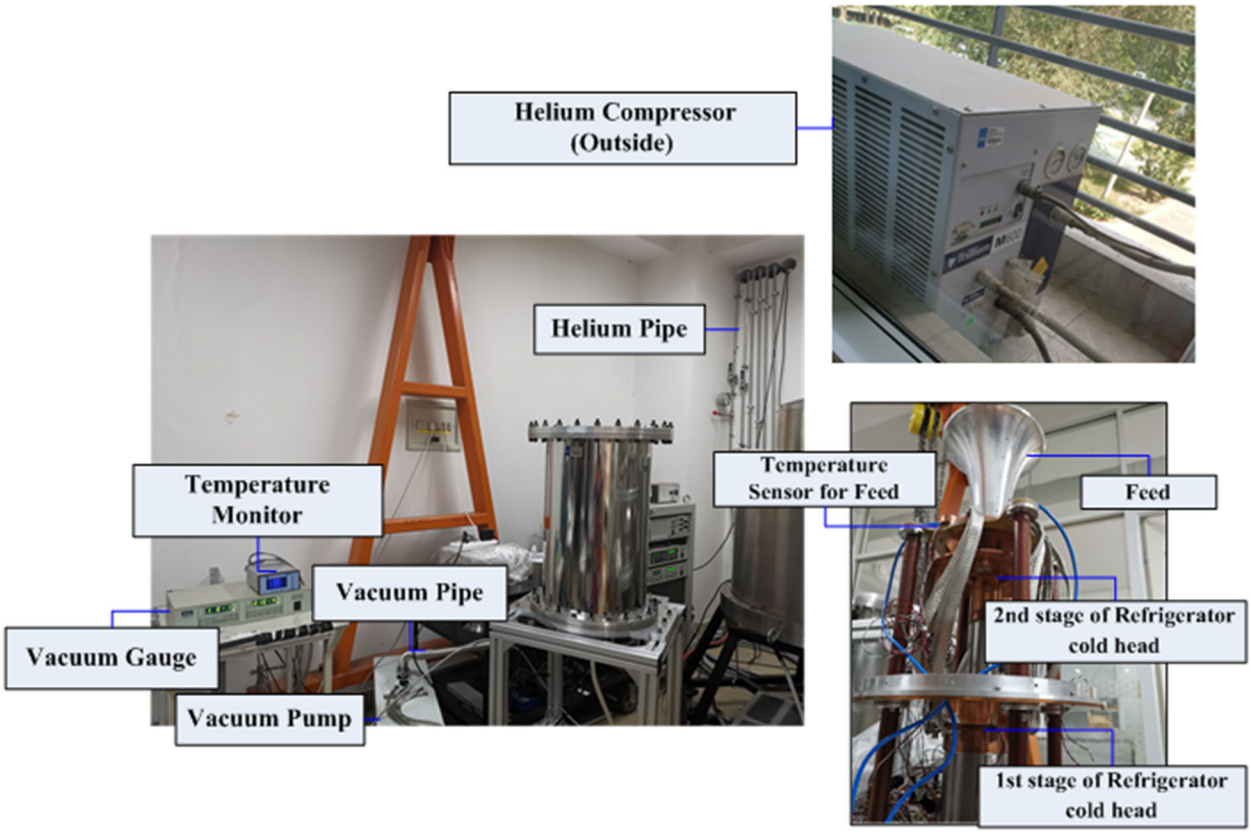

FIGURE 16. Measurement set up for Cryogenic QRFH.

FIGURE 17. Measured the Cryogenic QRFH temperature results.

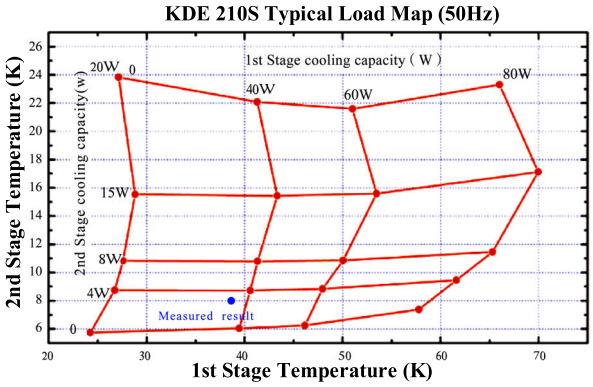

FIGURE 18. Measured heat result for 10: 1 bandwidth feed refrigerator.

The temperature on the baseplate of the thermal shield is 207 K and the baseplate of feed is 45 K. The inner diameter of the G10 supporters is 20 mm, the outer diameter of the G10 supporters is 24 mm, and the height is 210 mm. With four supporters used, by adopting Eq.(4), the value of conductive heat for H_2 was calculated as 0.124 W. By adding these two heats by using Eq.(5), the 1st stage total conductive heat ($H_{Conduction}$) can be predicted as 0.236 W.

2) ESTIMATING THERMAL LOAD DUE TO RADIATION

To determine the net exchange of radiant energy between two surfaces, three key elements must be considered, i.e. the geometry of the two surfaces (inner and outer), the temperatures of the inner surfaces and the emissivity of the surfaces' areas. In a practical measurement, the geometry of most systems is difficult to obtain accurate values. However, to estimate the radiation load for the size of the refrigerator, the following equation is often used [26]. All the area of surfaces were predicted by Solid Works software in this case.

$$Q = \frac{\sigma A_1 (T_2^4 - T_1^4)}{\frac{1}{\varepsilon_1} + \frac{A_1}{A_2}(\frac{1}{\varepsilon_2} - 1)} watts \tag{6}$$

where:

Q = radiation heat transfer, Watts
A_1 = area of inner surface, m^2
A_2 = area of outer surface, m^2
T_1 = temperature of inner surface, K
T_2 = temperature of outer surface, K
ε_1 = emissivity of the inner surface
ε_2 = emissivity of the inner surface
σ = 5. 74∗10^{-8} Watts/m^2K

The sources of radiant heat are obtained from the 1st stage of the Refrigerator cold head and the 2nd stage of the Refrigerator cold head.

$$\text{1st stage} \quad Q_{radiation} = Q_1 + Q_2 + Q_3 \tag{7}$$

Q_1 is radiant heat between the surface of the 300 K Vacuum Window and the 45 K inner surface Feed.

Q_2 is radiant heat between the area of the 300 K Dewar and the area of the 207 K Thermal Shield.

Q_3 is radiant heat between the area of the 207 K Thermal Shield and the 45 K outer surface Feed.

a: 1st STAGE OF REFRIGERATOR COLD HEAD: Q_1

A number of parameters need to be set before the measurement for the 1st stage is performed, such as the temperature of the Vacuum Window, *T2*, is set to 300 K in this case, the inner Feed, *T1*, is 45 K, the area of the Vacuum Window Mylar, *A2*, is 0.097264 m^2 and the area of inner Feed, *A1*, is 0.047861m^2. In addition, the feed was manufactured using anodized aluminum, where the emissivity of the inner surface, ε_1, is 0.97 [29]–[37], the emissivity of the outer surface, ε_2, is 1 [29]–[37] and the material is Mylar film. By adopting Eq.(6), the radiant heat Q_1 is 21. 63W from the Vacuum Window to the inner feed.

b: 1st STAGE OF REFRIGERATOR COLD HEAD: Q_2

The temperature of the Dewar is 300 K (T_2) and the Thermal Shield is 207 K (T_1). The area of the Dewar inner is 0.677 m^2, the area of the Dewar baseplate is 0.1051m^2, A_2 is 0.782 m^2 (0.677+0.105), the surface of the Thermal Shield outer is 0.377m^2, the surface of the Thermal Shield baseplate is 0.061 m^2, A_1 is 0.438m^2(0.377+0.061). The inner Thermal Shield is nickel-plated copper, and the emissivity of the inner surface, $\varepsilon 1$, is 0.05 [29]–[37], the outer Thermal Shield is stainless steel 304, and the emissivity of the outer surface, $\varepsilon 2$, is 0.16 [29]–[37]. Again, by using Eq.(6), the radiant heat Q_2 can be obtained as 6. 86W from the Dewar to the Thermal Shield.

c: 1st STAGE OF REFRIGERATOR COLD HEAD: Q_3

The temperature of the Thermal Shield is 207 K (T_2) and the Feed is 45 K (T_1). The surface area of the thermal shield outer is 0.377m^2, the surface area of the thermal shield baseplate, *A2*, is 0.061m^2. The surface area of the Feed outer, *A1*, is 0.049722 m^2. The inner Feed is nickel-plated copper, and the emissivity of the inner surface, $\varepsilon 1$, is 0.97 [26], [27], [29]–[33]. The outer Thermal Shield is stainless steel 304, and the emissivity of the outer surface, $\varepsilon 2$, is 0.05 [26], [27], [29]–[33]. By using Eq.(6), the radiant heat, Q_3, can be found to be 1. 64 W from the Thermal Shield to the Feed. Finally, the total radiant heat (1ststage $Q_{radiation}$) is 30. 13W (21.63 W+6.86 W+1.64 W) on the 1st stage of the Refrigerator cold head, which is found by adding all the radiant heats using Eq.(7). It can be concluded that, the calculated refrigerator heat for 10:1 bandwidth feed is 30.366 W (0.236 W+30.13W) on the 1st stage of the Refrigerator cold head. The calculated value is near to the measured result (37 W) on the 1st stage of the Refrigerator cold head.

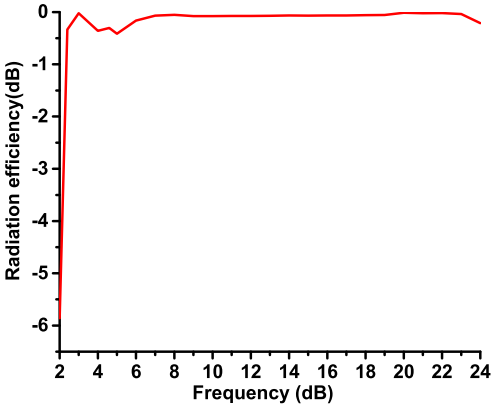

FIGURE 19. The calculated radiation efficiency.

Fig.19 shows the radiation efficiency (ohmic loss) [11] of the design, which was calculated using CST Microwave Studio. It is clearly seen that the radiation efficiency is between -0.04 and -0.4 dB at most frequency bands. From the measured physical temperature for the cryogenic QRFH feed, which is c. 45 K (see Table 5: Feed: 15088-2123-D and 17043-4307-C), we can predict the QRFH noise temperature from the equation below [38], [39]:

$$T_e = (L - 1) \times T_0 \tag{8}$$

T_e : Noise temperature; L: ohmic loss; T_0: physical temperature

For the radiation efficiency of the feed, the main factor is ohmic loss. Based on the radiation efficiency performance, Fig.20 is produced by using Eq. (8) to show the noise contribution that encompasses the working frequency band at room and cryogenic temperature. To sum up, the physical temperature of the QRFH level achieved is less than 45 K. It is noticeable that at cryogenic temperature 45K, the noise temperature range between 0.146K to 4.5K while at room temperature it varies between 1K to 30K. At the frequency band from 7 GHz to 23 GHz, the noise temperature is less than 0.83 K and 5.53 K for cryogenic and room temperature respectively. The calculated refrigerator heat from the simulations is close to the measured result. The performance of the QRFH is demonstrated applicable to be a feed option in a Square Kilometre Array reflector antenna. Fig.21 shows

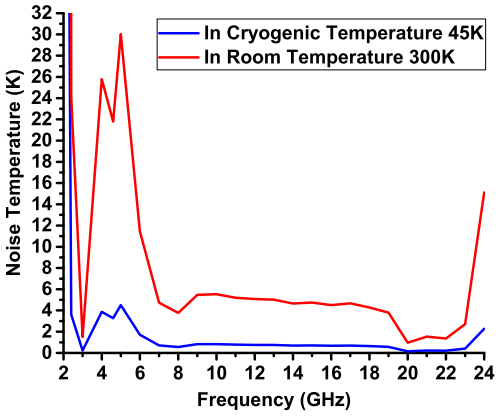

FIGURE 20. The calculated QRFH Noise contribution in different frequency bands.

FIGURE 21. SKA dish prototype with location of the proposed feed.

that the feed will be implemented into an SKA dish prototype with a diameter of 15 m for the main reflector and 5.2 m for the sub-reflector. Currently, this SKA dish is located in Shijia Zhuang, China and was manufacture by JLRAT [40].

V. CONCLUSION

This paper presents the optimization and realization of a 10:1 bandwidth cryogenic Quadruple-Ridged Flared Horn design for reflector antennas applicable in future wideband radio telescopes. The sunk profile, L-shaped matching block and, in particular, the probe inner conductor of the horn feed are studied and the cryogenic feed performance is also analyzed. The feed exhibits good impedance matching and radiation pattern performance over 10:1 bandwidth. By adopting the sunk curve profile, the design's phase center of the radiation patterns become more stable and concentrated. Therefore, more constant beamwidth and more symmetrical radiation patterns have been obtained. Two probes are designed by using the multiple matching rings cascade method, which eliminated the standing wave discontinuity at a certain point of a frequency band and resulted in good 50 Ω impedance matching of the four-ridged horn with broadband characteristics to up to 10:1 bandwidth. The reflection coefficient measured is less than 10dB and cross coupling is lower than -25 dB, which both agree with the simulated results. The whole QRFH was manufactured using aluminum alloy 8050 with relatively small horn apertures. It is easy to reduce the size of the vacuum window and thermal load in the cooling environment, and the construction for manufacturability, stability, and compatibility with cryogenic cooling. The noise temperature contribution of the feed predicted is less than 0.83 K at most working frequency bands, while the antenna aperture efficiency is above 55% over 2.4 to 24 GHz for the two ports. Consequently, the light and compact design facilitates cooling of the entire feed, which reduces receiver system noise temperature to obtain higher sensitivity. Meanwhile, this design could reduce the number of receivers for SKA reflectors, maintenance difficulties and cost, especially, in face of operating thousands of dishes. The 10:1 Bandwidth Cryogenic QRFH presented in this paper for use in an SKA dish prototype for carrying out astronomical observations will be promising feed option for the SKA currently in its construction stage.

ACKNOWLEDGEMENT

The authors would like to thank D. Li and N. Zhang from the 54th Research Institute of China Electronics Technology Group Corporation, who gave us assistancein the antenna measurements. They would also like to thank Dr. N. J. McEwan and J. Wang who provided insightful opinions about the presented work.

REFERENCES

[1] *Square Kilometre Array*. Accessed: Feb. 2, 2020. [Online]. Available: http://www.skatelescope.org/
[2] B. Peng *et al.*, "Preparing for the SKA: The Chinese perspectives," *Sci. Sinica*, vol. 47, no. 12, 2017, Art. no. 129501.
[3] Y. Ma, B. Billade, and Z. Z. Abidin, "Quad-ridge flared horn feed design and analysis for WBSPF in radio telescope," in *Proc. Ind Gen. Assem. Sci. Symp. Int. Union Radio Sci. (URSI GASS)*, Montreal, QC, USA, Aug. 2017, pp. 1–4.
[4] W. A. Imbriale and A. Akgiray, "Performance of a quad-ridged feed in a wideband radio telescope (EuCAP)," in *Proc. 5th Eur. Conf. Antennas Propag. (EUCAP)*, Rome, Italy, 2011, pp. 662–665.
[5] A. Akgiray, S. Weinreb, W. A. Imbriale, and C. Beaudoin, "Circular quadruple-ridged flared horn achieving near-constant beamwidth over multioctave bandwidth: Design and measurements," *IEEE Trans. Antennas Propag.*, vol. 61, no. 3, pp. 1099–1108, Mar. 2013.
[6] A. Akgiray, "New technologies driving decade-bandwidth radio astronomy: Quad-ridged flared horn & compound-semiconductor LNAs," Ph.D. dissertation, California Inst. Technol., Pasadena, CA, USA, 2013. Accessed: Dec. 30, 2019. [Online]. Available: https://thesis.library.caltech.edu/7644/1/Akgiray_PhDThesis_FinalVersion.pdf
[7] B. Dong, J. Yang, J. Dahlstrom, J. Flygare, M. Pantaleev, and B. Billade, "Optimization and realization of quadruple-ridge flared horn with new spline-defined profiles as a high-efficiency feed from 4.6 GHz to 24 GHz," *IEEE Trans. Antennas Propag.*, vol. 67, no. 1, pp. 585–590, Jan. 2019.
[8] J. Shi, S. Weinreb, W. Zhong, X. Yin, and M. Yang, "Quadruple-ridged flared horn operating from 8 to 50 GHz," *IEEE Trans. Antennas Propag.*, vol. 65, no. 12, pp. 7322–7327, Dec. 2017.
[9] B. Billade, J. Flygare, M. Dahlgren, B. Wastberg, and M. Pantaleev, "A wide-band feed system for SKA band 1 covering frequencies from 350–1050 MHz," in *Proc. 10th Eur. Conf. Antennas Propag. (EuCAP)*, Apr. 2016, pp. 1–3.
[10] J. Yang, J. Flygare, M. Pantaleev, and B. Billade, "Development of quadruple-ridge flared horn with spline-defined profile for band b of the wide band single pixel feed (WBSPF) advanced instrumentation programme for SKA," in *Proc. IEEE Int. Symp. Antennas Propag. (APSURSI)*, Jun. 2016, pp. 1345–1346.

[11] J. Yang, M. Pantaleev, P.-S. Kildal, B. Klein, Y. Karandikar, L. Helldner, N. Wadefalk, and C. Beaudoin, "Cryogenic 2–13 GHz eleven feed for reflector antennas in future wideband radio telescopes," *IEEE Trans. Antennas Propag.*, vol. 59, no. 6, pp. 1918–1934, Jun. 2011.
[12] R. Gawande and R. Bradley, "Towards an ultra wideband low noise active sinuous feed for next generation radio telescopes," *IEEE Trans. Antennas Propag.*, vol. 59, pp. 1945–1953, Jun. 2011.
[13] G. Cortes-Medellin, "Non-planar quasi-self-complementary ultra-wideband feed antenna," *IEEE Trans. Antennas Propag.*, vol. 59, no. 6, pp. 1935–1944, Jun. 2011.
[14] J. Flygare, B. Dong, J. Yang, L. Helldner, M. Dahlgren, J. Chengjin, M. Pantaleev, G. Hovey, and J. Conway, "Wideband single pixel feed system over 4.6–24 GHz for the square kilometre array," in *Proc. Int. Conf. Electromagn. Adv. Appl. (ICEAA)*, Granada, Spain, Sep. 2019, pp. 0630–0635.
[15] J. Flygare, "A wideband quad-ridge flared horn feed design for the square kilometre array band 1 antenna design, simulation and measurement," M.S. thesis, Dept. Fundam. Phys., Chalmers Univ. Technol., Gothenburg, Sweden, 2016. Accessed: Dec. 30, 2019. [Online]. Available: https://pdfs.semanticscholar.org/21e8/69241ef4f1165ca93f745a427ed69f9b9932.pdf
[16] A. R. Mallahzadeh, A. A. Dastranj, and S. Akhlaghi, "Quad-ridged conical horn antenna for wideband applications," *Int. J. RF Microw. Comput.-Aided Eng.*, vol. 19, no. 5, pp. 519–528, Sep. 2009.
[17] B. Solak, M. Secmen, and A. Tekin, "The design of a high gain dual-polarized quad-ridged circular horn antenna for wideband EMC test applications," *ACES J.*, vol. 33, no. 9, pp. 1009–1017, Sep. 2018.
[18] F. Yang, B. Du, J. Ma, Y. Wu, Y. He, and D. Li, "Development of a broadband wide-angle quad-ridged flared horn," in *Proc. Int. Conf. Microw. Millim. Wave Technol. (ICMMT)*, May 2019, pp. 1–3, doi: 10.1109/icmmt45702.2019.8992225.
[19] J. Flygare and M. Pantaleev, "Dielectrically loaded quad-ridge flared horn for beamwidth control over decade bandwidth–optimization, manufacture, and measurement," *IEEE Trans. Antennas Propag.*, vol. 68, no. 1, pp. 207–216, Jan. 2020.
[20] D. T. Al-Zuhairi, J. M. Gahl, and N. E. Islam, "Compact dual-polarized quad-ridged UWB horn antenna design for breast imaging," *Prog. Electromagn. Res. C*, vol. 72, pp. 133–140, Mar. 2017.
[21] F. Yang, D. Li, B. Du, Y. Wu, and Y. He, "Development of a 6-18 GHz quad-ridged flared horn," in *Proc. IEEE Asia–Pacific Conf. Antennas Propag. (APCAP)*, doi: 10.1109/apcap.2018.8538284.
[22] G. Tsandoulas and G. Knittel, "The analysis and design of dual-polarization square-waveguide phased arrays," *IEEE Trans. Antennas Propag.*, vol. 21, no. 6, pp. 796–808, Nov. 1973.
[23] M. H. Chen, G. N. Tsandoulas, and F. G. Willwerth, "Modal characteristics of quadruple-ridged circular and square waveguides (Short Papers)," *IEEE Trans. Microw. Theory Techn.*, vol. 22, no. 8, pp. 801–804, Aug. 1974.
[24] *CST Microwave Studio Software*. Accessed: Mar. 3, 2020. [Online]. Available: https://www.3ds.com/products-services/simulia/products/cst-studio-suite/electromagnetic-systems
[25] *TICRA GRASP Software*. Accessed: Mar. 3, 2020. [Online]. Available: www.ticra.com/software/grasp/
[26] G. Behrens, W. Campbell, D. Williams, and S. White. Guidelines for the Design of Cryogenic Systems. Mar. 1997. National Radio Astronomy Observatory? Accessed: Dec. 30, 2019. [Online]. Available: http://www.gb.nrao.edu/electronics/edir/edir306.pdf
[27] A. R. Kerr, N. J. Bailey, D. E. Boyd, and N. Horner. (Aug. 21, 1992). A Study of Materials for a Broadband Millimeter-Wave Quasi-Optical Vacuum Windows. National Radio Astronomy Observatory. Accessed: Dec. 30, 2019. [Online]. Available: http://legacy.nrao.edu/alma/memos/html-memos/alma090/Memo090.pdf
[28] *CSIC Pride Cryogenic Technology Company, Product Manual*. Accessed: Dec. 30, 2019. [Online]. Available: http://www.724pridecryogenics.com/en/product1.asp?bigid=99
[29] M. A. Bramson. *Infrared Radiation, A Handbook for Applications*. New York, NY, USA: Plenum, 2013.
[30] W. L. Wolfe and G. J. Zissis, "The infrared handbook," Dept. Navy, Office Naval Res., Washington, DC, USA, Tech. Rep., 1989. Accessed: Feb. 5, 2020. [Online]. Available: https://trove.nla.gov.au/work/8887950
[31] R. P. Madding, *Thermographic Instruments and Systems*. Madison, WI, USA: Univ. Wisconsin, Extension, Dept. Eng. Appl. Sci., 1979.
[32] W. L. Wolfe, "Handbook of military infrared technology," Dept. Navy, Office Naval Res., Environ. Res. Inst. Michigan, Austin, TX, USA, Tech. Rep. 1985-06, 1985.
[33] A. M. Jones, I. E. Smith, and S. D. Probert, "External thermography of buildings and structures as a means of determining their heat losses," *Proc. SPIE*, vol. 0110, pp. 14–16, Nov. 1977.
[34] P. Pettersson, *Thermography of Buildings*. Stockholm, Sweden: Swedish Building Research Institute, 1972.
[35] J. Vlcek, "A field method for determination of emisivity with imaging radiometers," *Photogramm. Eng. Remote Sens.*, vol. 48, no. 4, pp. 609–614, Apr. 1982. Accessed: Dec. 30, 2019. [Online]. Available: https://pdfs.semanticscholar.org/ae1c/2fa23cd643f4be0760e6d6a32a2647f85e17.pdf
[36] C. D. Kern, "Evaluation of infrared emission of clouds and ground as measured by weather satellites," Defence Documentation Center, New York, NY, USA, Tech. Rep. AD 617 417, 1964.
[37] C. Öhman, "Emittansmätningar med AGEMA E-box. Teknisk Rapport, AGEMA 1999," Emittance Meas. Using AGEMA E-Box, AGEMA, Sweden, Tech. Rep., 1999.
[38] P. M. David, *Microwave Engineering*, 4th ed. Hoboken, NJ, USA: Wiley, 2011, p. 503.
[39] S. Weinreb, "Cryogenic performance of microwave terminations, attenuators, absorbers, and coaxial cable," Nat. Radio Astron. Observatory, Charlottesville, VA, USA, Electron. Division Internal Rep. 223, 1982. Accessed: Dec. 30, 2019. [Online]. Available: http://www.gb.nrao.edu/electronics/edir/edir223.pdf
[40] *SKA Prototype Dish*. Accessed: Mar. 3, 2020. [Online]. Available: https://www.skatelescope.org/news/first-ska-prototype-dish-assembled/

YUE MA was born in Tangshan, Hebei, China, in 1986. She received the bachelor's degree (Hons.) in electrical and electronic engineering from the University of Bradford, U.K., in 2009, and the master's degree (Hons.) in electrical and electronic engineering from the University of Bradford, U.K., in 2010. Her research field covers the mobile and satellite communication antenna studies that includes RFID passive tag design at Europe UHF band, MIMO mobile handset antenna designs, CPW, UWB, phased array antennas for wireless communication applications in U.K. Since 2013, she has been working at the development on wide band single pixel feed, phased array feed, low noise amplifier, filter designs for the square kilometre array radio telescope in National Astronomical Observatories, Chinese Academy of Sciences. In 2017, she received the Young Scientists Award in the 32nd International Union of Radio Science General Assembly and Scientific Symposium (URSI 2017 GASS).

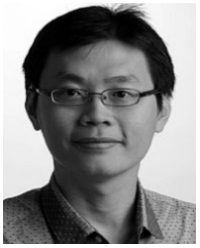

CHAN HWANG SEE (Senior Member, IEEE) received the B.Eng. degree (Hons.) in electronic, telecommunication, and computer engineering and the Ph.D. degree from the University of Bradford, U.K. He is an Associate Professor and the Head of Electrical Engineering and Mathematics with the School of Engineering and the Built Environment, Edinburgh Napier University, U.K. Previously, he was a Senior Lecturer (Programme Leader) in electrical & electronic engineering with the School of Engineering, University of Bolton, U.K. He is also a Visiting Research Fellow with the School of Engineering and Informatics, University of Bradford, U.K. Prior to this, he was a Senior Research Fellow with the Antennas and Applied Electromagnetics Research Group, University of Bradford. His research interests cover wireless sensor network system design, computational electromagnetism, antennas, and acoustic sensor design. He has published over 200 peer-reviewed journal articles and conference papers in the areas of antennas, computational electromagnetics, microwave circuits, and wireless sensor system designs. He is a coauthor for one book and three book chapters. He was a recipient of two Young Scientist Awards from the International Union of Radio Science (URSI) and Asia-Pacific Radio Science Conference (AP-RASC), in 2008 and 2010, respectively. He was awarded a certificate of excellence for his successful Knowledge Transfer Partnership (KTP) with Yorkshire Water on the design and implementation of a wireless sensor system for sewerage infrastructure monitoring, in 2009. He is a Chartered Engineer and a Fellow of the Institution of Engineering and Technology. He is also a Fellow of the Higher Education Academy and Associate Editor for IEEE Access.

FENG PANG received the Ph.D. degree in astronomical of techniques and methodology from the National Astronomical Observatories, Chinese Academy of Sciences, Beijing, China, in 2017. Since 2010, he has been a Senior Engineer with the National Astronomical Observatories, Chinese Academy of Sciences. His research interests include satellite communication, navigation, and radio astronomy.

DI WU was born in Beijing, in 1989. She received the B.E degree of mechanical engineering and automation and the M.E degree of mechatronic engineering from the Beijing Information Science and Technology University, in 2011 and 2014, respectively. Since 2014, she has been with the National Astronomical Observatories of China, Chinese Academy of Sciences, mainly work on the analysis of Dewar design and thermal load.

DONGLIANG LIU was born in 1983. He received the B.S. degree in electronic and information engineering from Beijing Jiao Tong University, China, in 2006 and the Ph.D. degree in astronomical of techniques and methodology from the National Astronomical Observatories, Chinese Academy of Sciences, Beijing, China, in 2011. Since 2012, he has been a Senior Engineer with the National Astronomical Observatories, Chinese Academy of Sciences. His research interests include the development of digital backend systems for radio telescope and the related signal and system analysis.

ZUHAIRIAH ZAINAL ABIDIN received the Ph.D. degree from Bradford University, U.K., in 2011. She was a Principal Researcher with the Research Center for Applied Electromagnetics (EMCenter), Universiti Tun Hussein Onn Malaysia. She has authored and coauthored numbers of journals and proceedings. Her research interests include MIMO antenna, printed microstrip antenna, wearable antennas, electromagnetic bandgap (EBG) for wireless and mobile, and high-speed digital circuit's applications.

SIMEON KEATES received the M.A. and Ph.D. degrees in engineering from the Department of Engineering, University of Cambridge, Cambridge, U.K. He is currently the Dean of the School of Engineering and the Built Environment, Edinburgh Napier University, Scotland. Previously, he was the Deputy Pro Vice Chancellor with the Faculty of Engineering and Science, University of Greenwich, London, U.K., where he is responsible for strategic management of Engineering and also for industrial engagement. Prior to this, he was the Head of the School of Engineering, Computing and Applied Mathematics, University of Abertay Dundee, Dundee, Scotland, and an Associate Professor with the IT University of Copenhagen, Copenhagen, Denmark, where he lectured in the Design and Digital Communication study line. He was an Industrial Research Fellow with the Engineering Design Centre, University of Cambridge, supported by the Royal Mail. He joined the Accessibility Research Group, IBM TJ Watson Research Center. He was with ITA Software as a Usability Lead designing interfaces for Air Canada. He also has an extensive history of consultancy, with clients including Royal Mail, the U.S. Social Security Administration, the U.K. Department of Trade and Industry, Danish Broadcasting Corporation (Danske Radio) and Lockheed Martin. He is a Fellow of the Institution of Engineering and Technology and Senior Fellow of the Higher Education Academy. He was the Chair of HCI.

BO PENG received the Ph.D. degree from the Beijing Astronomical Observatories, Chinese Academy of Sciences, in 1993. He has been working at radio astronomy research and technology development on large sky survey, transient phenomenon, giant radio galaxies, space weather and radio telescope instrumentation. He joined the global cooperation on the planned largest radio telescope array Square Kilometre Array (SKA) Project, in 1993, conducting the first SKA site survey on Radio Frequency Interferometer (RFI) measurements, in 1994. He is one of the key persons to initiate, develop and lead the largest single dish Five-hundred-meter Aperture Spherical Radio Telescope (FAST). He was the group founding leader of Large Telescope in 1994, becomes the Board member of the international SKA Project in 1999, and Director of the CAS Key Laboratory of FAST, in 2018.

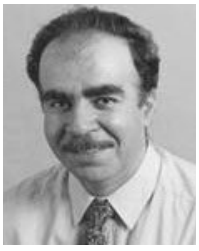

RAED A. ABD-ALHAMEED (Senior Member, IEEE) received the B.Sc. and M.Sc. degrees from Basrah University, Basrah, Iraq, in 1982 and 1985, respectively, and the Ph.D. degree from the University of Bradford, West Yorkshire, U.K., in 1997, all in electrical engineering. He is currently a Professor of electromagnetic and radio frequency engineering with the University of Bradford, U.K. He has long years' research experience in the areas of radio frequency, signal processing, propagations, antennas and electromagnetic computational techniques. He has published over 500 academic journal articles and conference papers. He is a coauthors of three books and several book chapters. At the present, he is the Leader of radio frequency, propagation, sensor design and signal processing, in addition to leading the Communications Research Group for years within the School of Engineering and Informatics, Bradford University, U.K. He is a Principal Investigator for several funded applications to EPSRCs and leader of several successful knowledge Transfer Programs, such as with Arris (previously known as Pace plc), Yorkshire Water plc, Harvard Engineering plc, IETG Ltd., Seven Technologies Group, Emkay Ltd., and Two World Ltd. He has also been a co-investigator in several funded research projects, including H2020 MARIE Skłodowska-CURIE ACTIONS, Innovative Training Networks (ITN) Secure Network Coding for Next Generation Mobile Small Cells 5G-US, Nonlinear and demodulation mechanisms in biological tissue, Department of Health, Mobile Telecommunications, and Health Research Program, and assessment of the potential direct effects of cellular phones on the nervous system (EU: collaboration with sic other major research organizations across Europe. His research interests include computational methods and optimizations, wireless and mobile communications, sensor design, EMC, beam steering antennas, Energy efficient PAs, and RF predistorter design applications. He is a Fellow of the Institution of Engineering and Technology and the Higher Education Academy, and a Chartered Engineer. He was awarded the business Innovation Award for his successful KTP with Pace and Datong companies on the design and implementation of MIMO sensor systems and antenna array design for service localizations. He is the Chair of several successful workshops on Energy Efficient and Reconfigurable Transceivers (EERT): Approach towards Energy Conservation and CO2 Reduction that addresses the biggest challenges for the future wireless systems. He has also appointed as a Guest Editor for the *IET Science, Measurements, and Technology Journal in 2009 and 2012. He is also a Research Visitor for Wrexham University, Wales, since September 2009, covering the wireless and communications research areas.*